Theory of Giant Electromechanical Response from Ferroelectric Bilayers with Polydomain Structures due to Interlayer and Interdomain Coupling

R. Mahjoub,[1] S. P. Alpay,[2] and V. Nagarajan[1,*]

[1]School of Materials Science and Engineering, University of New South Wales, Sydney, New South Wales 2052, Australia
[2]Materials Science and Engineering Program and Institute of Materials Science, University of Connecticut, Storrs, Connecticut 06269, USA

(Received 28 December 2009; published 2 November 2010)

The effect of interdomain ferroelastic coupling in ferroic multilayers is investigated theoretically. Specifically, we use nonlinear thermodynamics to analyze a heteroepitaxial ferroelectric $PbZr_xTi_{1-x}O_3$ (PZT) bilayer consisting of (001) tetragonal (T) PZT and (001) rhombohedral (R) PZT films. We predict for certain misfit strain regimes that interlayer and interdomain interactions lead to an adaptive domain structure in both the T and R layers and result in significant enhancements in the piezoelectricity compared to single-layer films. Our results demonstrate that electrostatic, magnetostatic, and elastic interactions in ferroic multilayers can be a generic route to generate ultrahigh susceptibilities.

DOI: 10.1103/PhysRevLett.105.197601 PACS numbers: 77.84.−s, 77.80.bn, 77.80.Dj

Multilayered thin film heterostructures wherein the individual constituents are stacked against each other under a restrictive two-dimensional geometry display a range of novel behavior in functional materials [1–6]. In multilayered ferroics, one other phenomenon that should be equally fascinating is the mechanical interaction across the multilayer interfaces. Ferroelastic interactions are generic to a broad class of ferroic materials wherein they typically lead to the formation of complex self-assembled (hierarchical) domain patterns in order to relax the excess elastic energy. A solid theoretical understanding and predictive modeling of the ferroelastic interactions across an interface will have a significant impact on the tailoring enhanced properties in a variety of ferroelastic nanostructures [7–9].

Recently, we demonstrated experimentally that such ferroelastic interactions in a ferroelectric bilayer lead to a giant piezoelectric response, up to 3 times larger than what is normally observed in constrained single-layered ferroelectric thin films [10]. Furthermore, Feigl *et al.* [11] show that the ferroelastic domain architecture in ferroelectric bilayers can be controlled by carefully engineering the defect structure of the interlayer interface. We note that the experimental [3,4,12–14] and theoretical [3,15–19] studies of ferroelectric multilayer heterostructures have mainly concentrated on ultrathin multilayers and superlattices consisting of monodomain ferroelectric and/or dielectric layers while there exists early work by Scott *et al.* that revealed interesting behavior in ferroelectric-ferroelectric multilayers [20]. In this Letter, we provide a comprehensive theoretical model that establishes the constitutive relations between layers, domains making up a particular layer, and domains across the interlayer interface through the application of the appropriate mechanical [21] and electrostatic boundary conditions and a rigorous tensorial analysis. The results predict that such interactions between the polydomain structures in a ferroic multilayer lead to a significant overall enhancement in the ferroic properties compared to single-layer films.

We consider here ferroelectric bilayers from the well-known $PbZr_xTi_{1-x}O_3$ (PZT) family consisting of a (001) PZT ($x < 0.5$) layer of thickness h_T and a (001) PZT ($x > 0.5$) layer of thickness h_R with tetragonal (T) and rhombohedral (R) crystal structures in bulk, respectively, on a thick (001) cubic substrate [Fig. 1(a)]. The total free energy of an individual layer that makes up a heterostructure as shown in Fig. 1 can be expressed very generally as

$$G_\Sigma = G_{\mathrm{LD}} - G_{\mathrm{elastic}} - G_{\mathrm{coupling}} - G_{\mathrm{electric}}. \quad (1)$$

Here, G_{LD} is the excess free energy due to the polarization $P_i (i = 1, 2, 3)$ in the ferroelectric state and can be expressed by a Landau-Devonshire (LD) expansion

$$G_{\mathrm{LD}} = \alpha_i P_i^2 + \alpha_{ij} P_i^2 P_j^2 + \alpha_{ijk} P_i^2 P_j^2 P_k^2, \quad (2)$$

where a_i, a_{ij}, a_{ijk} are the dielectric stiffness and higher order stiffness coefficients at constant stress. The elastic energy is given by $G_{\mathrm{elastic}} = 1/2\sigma_{ij} s_{ijkl} \sigma_{kl}$, where s_{ijkl} are the elastic compliances at constant polarization and σ_{ij} represents the stress field. G_{coupling} is the electromechanical energy due to the linear quadratic coupling of the

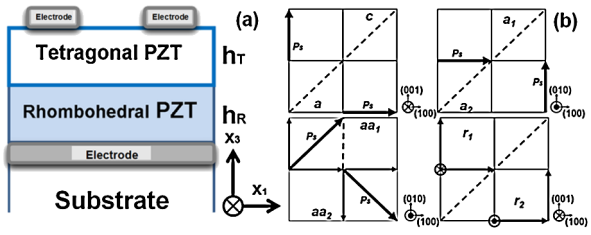

FIG. 1 (color online). (a) Schematic of the PZT bilayer system considered in this study and (b) the orientations of the polydomain structures.

self-strain of the ferroelectric phase transformation and the polarization. In its most general form, it can be expressed as $G_{\text{coupling}} = 1/2\sigma_{ij}Q_{ijkl}P_kP_l$, where Q_{ijkl} are the electrostrictive coefficients. The last term in Eq. (1) corresponds to the electrostatic energy of a short-circuited ferroelectric heterostructure that can be defined as $G_{\text{electric}} = P_iE_i + 1/2\varepsilon_0E_i^2$, where ε_0 is the permittivity of the vacuum and E_i is the electric field [22].

The total free energy per unit area of a bilayer structure will be the sum of the free energies of each layer weighted by their respective fractions. Superscripts T (tetragonal) and R (rhombohedral) are used for the macroscopic interlayer relations and 1 and 2 for the microscopic interdomain relations. Possible single and polydomain structures are defined through their spontaneous polarization vectors, as taken from Refs. [23,24]. The domain walls of $c/a/c/a$ and $r_1/r_2/r_1/r_2$ phases are along the [101] direction and those of $a_1/a_2/a_1/a_2$ and $aa_1/aa_2/aa_1/aa_2$ are perpendicular to the substrate interface. Interdomain interfaces of $a_1/a_2/a_1/a_2$ and $aa_1/aa_2/aa_1/aa_2$ are assumed parallel to [110] and [100]/[010], respectively. For simplicity, we assume in our calculations that the substrate–bottom electrode, bottom electrode–R-layer, and the R-T interlayer interfaces in Fig. 1(a) are free of misfit dislocations. This restriction can be easily removed by employing "effective" misfit strains in the R and T layers [21,25]. We adopt here a dense domain approach [26] such that the period of the polydomains is much smaller than the layer thickness. This is indeed confirmed by our experimental results on 70 nm layers that show the period of the ferroelastic domains to be ~10 nm [10].

In a bilayer polydomain ferroelectric heterostructure there are 36 stresses and electric-field components which need to be determined in terms of polarizations, strains, and domain fractions as independent variables. The unknown stresses and electric components can only be obtained by employing the microscopic as well as macroscopic boundary conditions. The microscopic boundary conditions, which arise from the twin boundary between two adjacent domains in a layer, consist of the requirement of elastic compatibility, mechanical equilibrium and electrostatics. The elastic compatibility between domains is given by $\varepsilon_{ij} = 1/2(u_{i,j} + u_{j,i})$ which leads to $\varepsilon_{ij}^1 = \varepsilon_{ij}^2$ ($ij = 11, 22, 12$) where u is the displacement, and the mechanical equilibrium given by $\sigma_{ij,j} = 0$ results in $\sigma_{ij}^1 = \sigma_{ij}^2$ ($ij = 13, 23, 33$). In the absence of free charges at the domain interfaces, $\nabla \cdot D = 0$ where D is the electric displacement field, and the continuity of the out-of-plane electric displacement yields $D_3^1 = D_3^2$. The continuity of the in-plane electric field required by $\nabla \times E = 0$ at domain interfaces leads to $E_i^1 = E_i^2$ ($i = 1, 2$). These microscopic conditions provide us with up to 18 equations. To implement the above microscopic requirements, crystallographic orientations of domain interfaces have to be taken into account by rotating all related vectorial and other higher-rank tensorial quantities of domains bearing in mind that each polydomain structure in the T and R layers will have a unique crystallographic relation. Schematics of polydomain configurations are shown in Fig. 1(b).

Macroscopic conditions include six equations obtained by the application of two-dimensional clamping to the average in-plane strains $\langle\varepsilon_{ij}\rangle = \varepsilon_{ij}^m$ ($ij = 11, 22, 12$) where ε_{ij}^m is the polarization-free misfit strain between the films and the substrate and $\varepsilon_{ij} = -\partial G/\partial\sigma_{ij} = Q_{ijkl}P_kP_l + s_{ijkl}\sigma_{kl}$ is the strain field in each domain. They also include the vanishing of the average out-of-plane stresses $\langle\sigma_{ij}\rangle = 0$ ($ij = 33, 23, 13$) which yields six more equations. The electrostatic requirements at the interface between ferroelectric films constitute the last six macroscopic conditions. Charge continuity leads to

$$\varepsilon_0\langle E_3^T\rangle + \langle P_3^T\rangle = \varepsilon_0\langle E_3^R\rangle + \langle P_3^R\rangle \tag{3}$$

and the in-plane electrical fields in the T and the R layers have to obey

$$\langle E_i^T\rangle = \langle E_i^R\rangle \qquad (i = 1, 2), \tag{4}$$

$$\langle E_i^T\rangle + \langle E_i^R\rangle = E_i^{\text{app}} \qquad (i = 1, 2, 3), \tag{5}$$

where E_i^T and E_i^R are the internal electric-field vectors in the T and R layers, respectively, and E_i^{app} is the external applied electric field. As such, the out-of-plane components of electric fields are obtained as

$$\langle E_3^T\rangle = \frac{h_R}{(h_R + h_T)\varepsilon_0}(\langle P_3^R\rangle - \langle P_3^T\rangle) + E_3^{\text{app}}, \tag{6}$$

$$\langle E_3^R\rangle = -\frac{h_T}{(h_R + h_T)\varepsilon_0}(\langle P_3^R\rangle - \langle P_3^T\rangle) + E_3^{\text{app}}, \tag{7}$$

where P_3^T and P_3^R are the out-of-plane polarizations in the T and R layers, respectively. For the ferroelectric bilayer shown in Fig. 1, a total number of 100 permutations of possible pairs of phases must be investigated and compared with each other so that the equilibrium phases or phase mixtures can be identified in the T and the R layers. This can be achieved numerically for systems such as PZT for which there exist thermodynamic, elastic, dielectric, and electromechanical data [27]. Once the stability range of the polarization in both layers is established, it becomes possible to find the overall small-signal piezoelectric coefficients of the bilayer structure given by $d_{ij} = \partial\langle\varepsilon_{ij}\rangle/\partial E_i$.

We have considered two bilayer systems in our numerical analysis: $PbTiO_3$ (PTO)–$PbZr_{0.6}Ti_{0.4}O_3$ (PZT60/40) and PZT30/70–PZT70/30. The dielectric stiffness coefficients and other materials constants entering the calculations are taken from Refs. [27,28]. Polydomain misfit strain-temperature phase diagrams of the ferroelectric T and R layers of PTO–PZT60/40 structure with a thickness

ratio $h_T/h_R = 1$ are plotted in Figs. 2(a) and 2(b), respectively, and their respective single-layer phase diagrams are shown by dashed [Fig. 2(a) for PTO] and dotted [Fig. 2(b) for PZT60/40] lines. Interestingly, the shifts of the T and R layers transition points between the paraelectric phase, the c phase, and the $c/a/c/a$ and $a_1/a_2/a_1/a_2$ structures are in opposite directions. Moreover, in the T layer [Fig. 2(a)], the stability region of the $c/a/c/a$ structure increases in the compressive misfit strain region at the cost of the c phase. On the other hand, in the tensile region the stability of the $c/a/c/a$ polydomain decreases slightly in favor of the $a_1/a_2/a_1/a_2$ pattern. Furthermore, size induced effects can be checked in bilayers by varying the thickness ratios. Our results (not shown) predict that the shift of phase diagram, the reduction in the transition temperature, and its displacement towards the compressive region become more pronounced as the thickness of the R layer is increased. In Fig. 2(b), in contrast to the T layer, the minimum critical temperature of the R layer increases and shifts to the in-plane tensile region. Additionally, the stability of the $r_1/r_2/r_1/r_2$ pattern decreases with respect to those of the c phase and the $a_1/a_2/a_1/a_2$ structure and the narrow range of the $c/a/c/a$ pattern vanishes.

To understand the compositional effects, a Zr-rich bilayer consisting of PZT30/70– PZT70/30 (with $h_T/h_R = 1$) is studied, see Figs. 2(c) and 2(d). The dashed and the dotted lines in Figs. 2(c) and 2(d) correspond to the misfit strain-temperature phase diagrams of single-layer PZT30/70 and PZT70/30, respectively. Here, the shift of the critical temperature is more significant in the T layer and less pronounced in the R layer. A comparison of Figs. 2(c) and 2(a) that the phase diagrams of compositions with higher Ti content are more susceptible to shifts induced by increasing the thickness of the R layer, which we tie to the stronger self-strain components. Finally, when we restrict the simulations only to monodomain phases we indeed find that the system has an overall monoclinic polarized phase consistent with the findings based on first principles [29] where monoclinic r phase replaces the polydomain tetragonal $c/a/c/a$ and monoclinic $r_1/r_2/r_1/r_2$ phases for a considerable interval of misfit strain at room temperature.

The interlayer and interdomain electrostatic and elastic couplings are found to affect the energy landscape such that a small external field can remarkably disturb the energy wells. This results in sharp changes in the stationary points which represent the polarization components at equilibrium. This phenomenon is illustrated in Fig. 3. Figures 3(a) and 3(b) show the three-dimensional landscape of the bilayer energy surface in the absence and presence of a small electric field, respectively. The two-dimensional projections of the shallow energy wells are magnified in Figs. 3(c) and 3(d) and in the insets. The symmetry of the energy surface is clearly disturbed under the external electric field. The abrupt changes in polarizations in the R and T layers due to a small electric field are found to drive the enhancements in the piezoelectric response where the ensuing abrupt domain wall displacements will be accompanied by very large electromechanical properties. As a result the system, which is positioned on the verge of two competing polarization states, is able to alter the equilibrium polarization significantly to induce a large electromechanical response not only at the phase boundaries but also across an entire misfit range under a

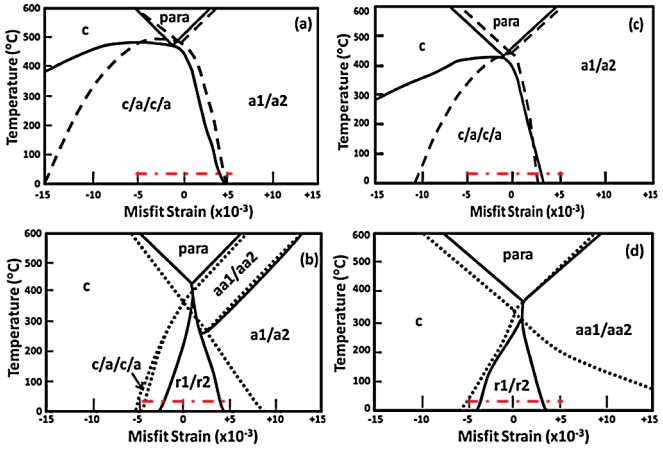

FIG. 2 (color online). Polydomain misfit strain-temperature phase diagram of short-circuited PTO–PZT60/40 (a),(b) and PZT30/70–PZT70/30 (c),(d) bilayer structures for $h_T/h_R = 1$. In each figure the solid line represents the case for the bilayer and dash–dotted line is for corresponding single layer. (a) PTO, (b) PZT60/40, (c) PZT30/70, (d) PZT70/30. The room temperature d_{33} peaks illustrated in Figs. 4 are located on the dash-dotted lines.

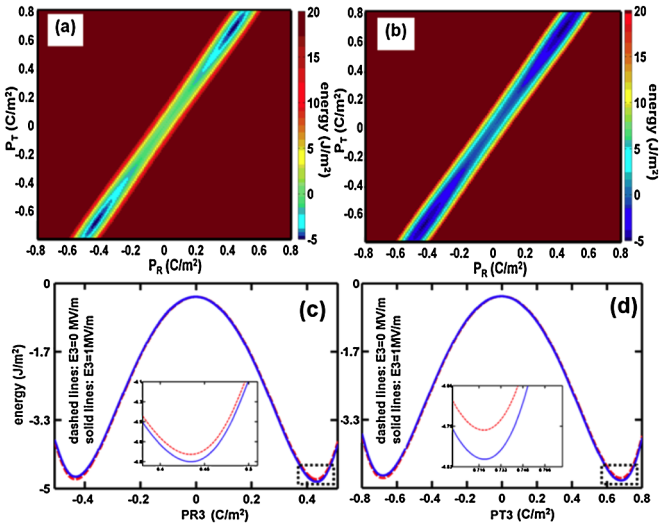

FIG. 3 (color online). The energy surfaces (per unit area) of a PTO-PZT60/40 system, in the absence (a) and in the presence of a small electric field (b). Dashed and solid lines in figures (c), (d) represent magnified two-dimensional projections of shallow energy wells in the absence and presence of external field. The ensuing abrupt changes in polarizations marked by dotted rectangles are enlarged and depicted in the insets.

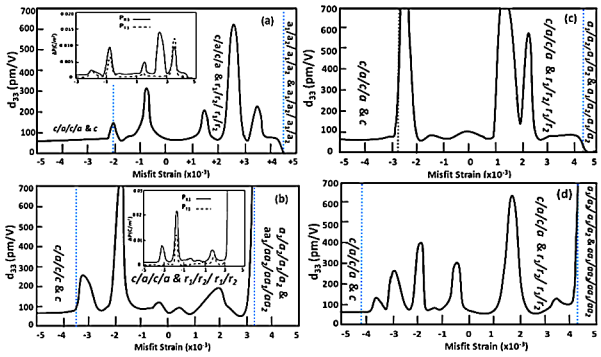

FIG. 4 (color online). Out-of-plane piezoelectric coefficient (d_{33}) of a short-circuited polydomain ferroelectric bilayer given in Fig. 1(a) at room temperature: (a) PTO and PZT60/40 with $h_T/h_R = 1$, (b) PZT30/70 and PZT70/30 with $h_T/h_R = 1$ [the insets to (a) and (b) depict the electric field induced change in the out-of-plane polarizations], (c) PTO and PZT60/40 with $h_T/h_R = 1/2$, and (d) PZT70/30 and PZT30/70 with $h_T/h_R = 1/2$. The vertical lines correspond to phase boundaries appearing in a room temperature snapshot of Fig. 2 with the misfits lying between -0.005 and $+0.005$ where mainly $r_1/r_2/r_1/r_2$ polydomains are found subjacent to $c/a/c/a$ phase.

reasonably small electric field (of the order of 10 kV/cm). This is shown in Figs. 4(a) and 4(b) for the PTO–PZT60/40 and PZT30/70–PZT70/30 systems, respectively, where the peaks in the numerically calculated room temperature d_{33} of bilayer structures match to the jumps observed in the computed change in polarization vs misfit strain plots [see corresponding insets to Figs. 4(a) and 4(b)].

The changes in the polarizations of the bilayer as a function of misfit strain imply that the electric-field induced $r_1/r_2/r_1/r_2$ polarization paths will also rotate, consistent with the previously reported findings [30]. Any change in the polarizations due to an applied electric field will induce a considerable change in the strain in both layers through the electrostatic and electromechanical interactions between the layers [see, e.g., Eqs. (6) and (7)].

The out-of-plane piezoelectric coefficients of bilayers with $h_T/h_R = 1/2$ are plotted in Figs. 4(c) and 4(d) for PTO–PZT60/40 and PZT30/70–PZT70/30, respectively. Critically, it is observed that peaks as large as 600 pm/V (compared to ~80 pm/V in the corresponding T single layer).

In summary, the theoretical model presented in this study predicts that the electrical and electromechanical interdomain and interlayer interactions lead to an order of magnitude increase in the piezoelectric properties of ferroelectric bilayers consisting of T and R layers, when compared to their single-layer constituents. The findings of this analysis can be extended to explain considerable improvements in ferroic properties reported in a number of multilayered ferroelectric systems [5,31].

This research is supported by an ARC Discovery Grant. High Performance Computing Center at the UNSW is acknowledged for providing the computational resources used in this work.

*Corresponding author.
nagarajan@unsw.edu.au

[1] M. N. Baibich *et al.*, Phys. Rev. Lett. **61**, 2472 (1988).
[2] S. S. P. Parkin *et al.*, Nature Mater. **3**, 862 (2004).
[3] N. Reyren *et al.*, Science **317**, 1196 (2007).
[4] M. Dawber *et al.*, Phys. Rev. Lett. **95**, 177601 (2005).
[5] H. N. Lee *et al.*, Nature (London) **433**, 395 (2005).
[6] C. v. Korff Schmising *et al.*, Phys. Rev. Lett. **98**, 257601 (2007).
[7] P. E. Vullum *et al.*, Adv. Mater. **19**, 4399 (2007).
[8] J. M. Pruneda *et al.*, Phys. Rev. Lett. **99**, 226101 (2007).
[9] L. J. Swartzendruber *et al.*, Phys. Rev. Lett. **64**, 483 (1990).
[10] V. Anbusathaiah *et al.*, Adv. Mater. **21**, 3497 (2009).
[11] L. Feigl *et al.*, J. Appl. Phys. **105**, 061607 (2009).
[12] F. A. Urtiev, V. G. Kukhar, and N. A. Pertsev, Appl. Phys. Lett. **90**, 252910 (2007).
[13] E. Bousquet *et al.*, Nature (London) **452**, 732 (2008).
[14] M. Dawber *et al.*, Adv. Mater. **19**, 4153 (2007).
[15] N. Sai, B. Meyer, and D. Vanderbilt, Phys. Rev. Lett. **84**, 5636 (2000).
[16] S. M. Nakhmanson, K. M. Rabe, and D. Vanderbilt, Phys. Rev. B **73**, 060101 (2006).
[17] M. B. Okatan, J. V. Mantese, and S. P. Alpay, Phys. Rev. B **79**, 174113 (2009).
[18] A. M. Bratkovsky and A. P. Levanyuk, Phys. Rev. B **66**, 184109 (2002).
[19] A. Artemev *et al.*, J. Appl. Phys. **103**, 074104 (2008).
[20] A. Q. Jiang *et al.*, J. Appl. Phys. **92**, 6756 (2002).
[21] R. Mahjoub *et al.*, J. Appl. Phys. **104**, 124103 (2008).
[22] M. J. Haun *et al.*, J. Appl. Phys. **62**, 3331 (1987).
[23] Y. L. Li *et al.*, J. Appl. Phys. **97**, 034112 (2005).
[24] V. G. Koukhar, N. A. Pertsev, and R. Waser, Phys. Rev. B **64**, 214103 (2001).
[25] Q. Y. Qiu, V. Nagarajan, and S. P. Alpay, Phys. Rev. B **78**, 064117 (2008).
[26] A. L. Roitburd, Phys. Status Solidi A **37**, 329 (1976).
[27] M. J. Haun *et al.*, Ferroelectrics **99**, 45 (1989); elastic compliances were taken from *Physics of Ferroelectrics*, edited by K. M. Rabe, C. H. Ahn, and J. M. Triscone (Springer, Berlin, 2007).
[28] V. G. Kukhar *et al.*, Phys. Rev. B **73**, 214103 (2006).
[29] C. Bungaro and K. M. Rabe, Phys. Rev. B **69**, 184101 (2004).
[30] L. Bellaiche, A. Garcia, and D. Vanderbilt, Phys. Rev. B **64**, 060103 (2001).
[31] M. P. Warusawithana *et al.*, Phys. Rev. Lett. **90**, 036802 (2003).